

Sensing Performance of Cooperative Joint Sensing-Communication UAV Network

Xu Chen, *Student Member, IEEE*, Zhiyong Feng, *Senior Member, IEEE*, Zhiqing Wei, *Member, IEEE*, Feifei Gao, *Fellow, IEEE*, and Xin Yuan, *Member, IEEE*

Abstract—We propose a novel cooperative joint sensing-communication (JSC) unmanned aerial vehicle (UAV) network that can achieve downward-looking detection and transmit detection data simultaneously using the same time and frequency resources by exploiting the beam sharing scheme. The UAV network consists of a UAV that works as a fusion center (FCUAV) and multiple subordinate UAVs (SU). All UAVs fly at the fixed height. FCUAV integrates the sensing data of network and carries out downward-looking detection. SUs carry out downward-looking detection and transmit the sensing data to FCUAV. To achieve the beam sharing scheme, each UAV is equipped with a novel JSC antenna array that is composed of both the sensing subarray (SenA) and the communication subarray (ComA) in order to generate the sensing beam (SenB) and the communication beam (ComB) for detection and communication, respectively. SenB and ComB of each UAV share a total amount of radio power. Because of the spatial orthogonality of communication and sensing, SenB and ComB can be easily formed orthogonally. The upper bound of average cooperative sensing area (UB-ACSA) is defined as the metric to measure the sensing performance, which is related to the mutual sensing interference and the communication capacity. Numerical simulations prove the validity of the theoretical expressions for UB-ACSA of the network. The optimal number of UAVs and the optimal SenB power are identified under the total power constraint.

Index Terms—Joint sensing-communication system, cooperative sensing, beam sharing, unmanned aerial vehicle network.

I. INTRODUCTION

Cooperative sensing unmanned aerial vehicle (UAV) network has been very promising in disaster rescue, surveillance, resource exploration, etc [2]. Due to unmanned feature and power restriction, UAVs need to achieve functions such as communication, environment sensing and flying status perception under load, volume and spectrum constraints. The utilization of the joint sensing-communication (JSC) technique on the UAV platform is a reasonable choice for the cooperative sensing UAV network, because it has advantages in load saving and spectrum reuse by sharing the same antennas, transceivers

and spectrum to achieve sensing and communication [3]. With the integration of the sensing data from multiple UAVs using the JSC techniques, the sensing zone of the network will be extended far beyond the radio propagation limit of single sensing platform [4]. Thus, with limited spectrum for radar sensing and communication, the cooperative JSC UAV network can finish detecting a large area in much shorter time and gather more environment information than an individual UAV does, which makes the network be more agile and decide on a larger picture.

The achievement of the JSC technique gains increasingly sufficient fundamentals. The communication spectrum has gradually occupied the frequency band that was dedicated to radar at first [4]. Digital signal processing techniques have been widely utilized both in sensing and communication transceivers [4], [5]. Thus, the spectrum and hardwares that are separately designed for sensing and communication have great potential for convergence [3].

The strong need and potential for the joint design of communication and sensing has motivated a number of important studies in the JSC technique. The approaches to realize the JSC system can be divided into three categories: time sharing, waveform co-design and beam sharing. Time sharing scheme has the intrinsic disadvantage that it does not allow simultaneous operation of sensing and communication, which will lead to the loss of detection target [6]. As for waveform co-design scheme, the communication direction is rigidly constrained by sensing direction. Therefore, the freedom of communication is severely reduced [7], [8]. On the contrary, the beam sharing scheme allows simultaneous operation of sensing and communication using different beams, which can carry out communication and sensing as freely as possible [1], [9]–[11]. The beam sharing scheme is based on the beamforming technology that has solid fundamentals. Monzingo and Miller proposed maximum signal-to-noise ratio (SNR) beamforming to generate optimal beam with the existence of strong noise [12]. Frost proposed linearly-constrained minimum variance beamforming that can generate the beamforming vector with linear complexity [13]. Shi and Feng proposed a two-step iterative beamforming algorithm to achieve beamforming of high performance [14]. Another fundamental aspect in JSC implementation is the JSC waveform. Traditional sensing waveform design concentrates on the waveforms with desirable autocorrelation properties. Linear frequency modulated (LFM) pulse signal, i.e., “chirp” signal, is a typical sensing waveform [15]. Exploiting the high SNR characteristics of radar signal, a bio-inspired radio frequency (RF) steganography scheme that

Part of related work was accepted by IEEE International Conference on Signal, Information and Data Processing (ICSIDP) 2019 [1]. Xu Chen, Z. Feng, Z. Wei and Xin Yuan are with Beijing University of Posts and Telecommunications, Key Laboratory of Universal Wireless Communications, Ministry of Education, Beijing 100876, P. R. China (Email: {chenxu96330, fengzy, weizhiqing, yuanxin}@bupt.edu.cn).

F. Gao is with Institute for Artificial Intelligence, Tsinghua University (THUAI), State Key Lab of Intelligent Technologies and Systems, Tsinghua University, Beijing National Research Center for Information Science and Technology (BNRist), Department of Automation, Tsinghua University Beijing, P. R. China (email: feifeigao@ieee.org).

Corresponding author: Zhiyong Feng, Zhiqing Wei

can conceal digital communication in linear chirp radar signals was proposed in [16]. Frequency modulated continuous wave (FMCW) is the typical continuous-wave sensing waveform [17]. In addition, the direct sequence spread spectrum (DSSS) waveform is also widely studied due to its features in information security and spectrum spread gains [18]. C. Sturm proposed an orthogonal-frequency-division-multiplexing (OFDM) symbol-based sensing processing technique to take advantage of temporal and frequency domain signal [19].

However, all the above works only study a single JSC unit or a single pair of JSC. Thus, in [1], we proposed a cooperative sensing performance metric of the JSC UAV network based on beam sharing scheme, but we were unable to put forward the proper antenna array model and beamforming algorithm. Moreover, we simplified the model by neglecting the mutual radar sensing interference and the guard distance between UAVs, which renders the proposed sensing performance metric less practical. Thus, in this paper, to enhance the concept of beam sharing JSC cooperative sensing UAV network we proposed in [1], we focus on the practical implementation of beam sharing JSC UAV network and further model the mutual sensing interference to analyze the sensing performance of cooperative JSC UAV network, which will offer guidance to the optimal deployment of the JSC UAV network, such as power allocation and the size of UAV network. The JSC UAV network consists of a UAV that works as the fusion center (FCUAV) and multiple subordinate UAVs (SU). All UAVs fly at the fixed height. UAVs carry out downward-looking sensing and integration of sensing data by generating a sensing beam (SenB) and a communication beam (ComB) with a novel JSC antenna array, respectively. The proper beamforming algorithm is also proposed. Because of the spatial orthogonality of communication and sensing, SenB and ComB can be easily formed orthogonally. SenB and ComB of each UAV share a total amount of available radio power. The average mutual sensing interference is modeled based on the radio propagation theory. The upper bound of average cooperative sensing area (UB-ACSA) is used to measure the cooperative sensing performance of the JSC UAV network [1], which is related to the mutual sensing interference and communication capacity. The main contributions of this paper are summarized as follows.

1. We design a novel JSC antenna array and present a corresponding iterative beamforming algorithm that can flexibly form SenB and ComB using multi-layer circular array and linear array, respectively. Communication and sensing can operate simultaneously utilizing the proposed antenna array.
2. We model the mutual sensing interference of the JSC UAV network, which can be used to evaluate the interference of the JSC UAV network.
3. We define and formulate UB-ACSA of the JSC UAV network as the cooperative sensing performance metric, taking into consideration the average mutual sensing interference. After the formula of UB-ACSA is validated numerically, we obtain the optimal number of UAVs and power allocation ratio of sensing beam power to total

TABLE I: Key parameters and abbreviations

Symbol	Description
FCUAV	The UAV acting as fusion center
SU	Subordinate UAV
MCA	Maximum cooperating area
MCR	Maximum cooperating range, x_Q
SZ	Sensing zone
ACSA	Average cooperative sensing area
UB-ACSA	The upper bound of ACSA, $S_{CSA}(M)$
ComA	Communication subarray of JSC array
SenA	Sensing subarray of JSC array
ComB	Communication beam
SenB	Sensing beam
SPR	Sensing power ratio, β_R
TxA	The transmitting antenna array of SenA
RxA	The receiving antenna array of SenA
S-C pair	The pair of FCUAV and an SU that is transmitting sensing data
STP	Successful transmission probability
R_g	The inner radius of MCA
R_{max}	Maximum effective sensing range
G_p	OFDM symbol-based radar processing gain
R_i	The distance between SU_i and FCUAV
h	The flying height of UAVs

available power.

The remaining parts of this paper are organized as follows. In Section II, we describe the cooperative JSC UAV network model, the beam sharing scheme, the design of JSC antenna, the corresponding beamforming algorithms, the JSC signal waveform, and the modeling of mutual sensing interference. Section III provides the closed-form expressions for minimum required signal-to-interference-and-noise ratio (SINR), the maximum sensing range of UAVs, maximum cooperative range (MCR), and UB-ACSA. Section IV formulates the outage capacity of the JSC UAV network as the communication performance metric. Subsequently, we provide the ultimate expression for MCR based on the outage capacity of the network. In section V, the numerical simulation of the previous theoretical results is presented. Section VI concludes this paper.

Notations: Bold uppercase letters denote matrices (i.e., \mathbf{M}); bold lowercase letters denote column vectors (i.e., \mathbf{v}); scalars are denoted by normal font (i.e., γ); the entries of vectors or matrices are referred to with parenthesis, for instance, the q th entry of vector \mathbf{v} is $\mathbf{v}(q)$, and the entry of the matrix \mathbf{M} at the m th row and q th column is $\mathbf{M}(m, q)$; \mathbf{I}_Q is the identity matrix with dimension $Q \times Q$. Also, matrix superscripts $(\cdot)^H$, $(\cdot)^*$ and $(\cdot)^T$ denote Hermitian transpose, complex conjugate and transpose, respectively. Besides, we use $(\cdot)^{-1}$ to denote inverse of matrix, $(\cdot)^\dagger$ to denote the pseudo-inverse of the matrix, $diag(\mathbf{v})$ to denote a diagonal matrix with the entries of \mathbf{v} on the diagonal, $E(\cdot)$ to denote the expectation of random variable, and $\lfloor \cdot \rfloor$ to denote the floor function.

II. SYSTEM MODEL

A. Model of Cooperative JSC UAV Network

We consider a cooperative JSC UAV network that conducts downward-looking detection and detection data communication simultaneously. As illustrated in Fig. 1, the network

consists of an FCUAV and M SUs, where all UAVs hover within a constrained two-dimensional (2D) plane at a fixed altitude h . Each UAV has an antenna array¹ that consists of a communication array (ComA) and a sensing array (SenA) to generate a ComB and a SenB, respectively. SenB is pointed downward to detect the targets on the ground (or the sea), and ComB is pointed to UAVs to transmit sensing data. Due to the significant difference between the sensing direction and the communication direction, ComB and SenB can be easily formed orthogonally and operate simultaneously to achieve beam sharing scheme. FCUAV integrates all the sensing data from SUs with ComB and detects targets simultaneously with SenB. SUs detect the targets with SenB while simultaneously transmitting the sensing data to FCUAV with ComB.

The antenna array of each UAV has available radio power P , i.e., the sum of SenB power and ComB power is P . The SenB power is given by

$$P_r = \beta_R P, \quad (1)$$

where β_R is defined as the sensing power ratio (SPR). The ComB power is thus $P_c = 1 - \beta_R P$. OFDM waveform is adopted as the communication and sensing waveform to achieve joint communication and sensing [4]. Time division multiple access (TDMA) is adopted by the JSC UAV network to exploit the same frequency band to transmit sensing data. To ensure that FCUAV integrates the intact sensing data of each SU, the communication capacity between each SU and FCUAV has to be larger than the generating rate of sensing data. Therefore, the distance between FCUAV and each SU must be smaller than MCR, denoted by x_Q . Each UAV also has a guard radius R_g for safety, within which no other UAVs can hover. Thus, SUs distribute within a concentric circle area centered at FCUAV, which is defined as the maximum cooperation area (MCA) whose inner and outer radii are R_g and x_Q , respectively.

To satisfy the constraints on the false alarm rate and the detection probability for effective sensing [20], each UAV has to decrease the loss of sensing signal power and reduce interference to other UAVs in order to maintain the minimum SINR of sensing [21]. Thus, there is the maximum sensing range for each UAV, which is denoted by R_{max} . As shown in Fig. 1, the region on the ground that the JSC UAV network has to detect is defined as the detected plane. The region in the detected plane that can be effectively detected² by a UAV is defined as the sensing zone (SZ) of the UAV. The maximum radius of SZ is determined by R_{max} and h . We propose the average union area of SZs of all UAVs to be the sensing performance metric of the JSC UAV network. The outage capacity of the links between SUs and FCUAV is defined as the communication performance metric of the JSC UAV network.

B. Beam Sharing Scheme and Design of JSC Antenna Array

The beam sharing scheme is used to realize communication and sensing simultaneously. Let (φ, θ) be a certain direction

¹All antenna elements are isotropic.

²i.e., the false alarm rate is below the maximum and detection probability is higher than the minimum.

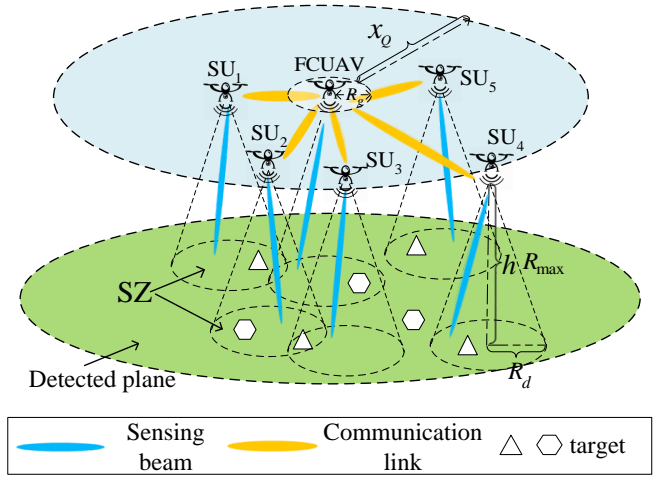


Fig. 1: JSC UAV cooperative sensing network

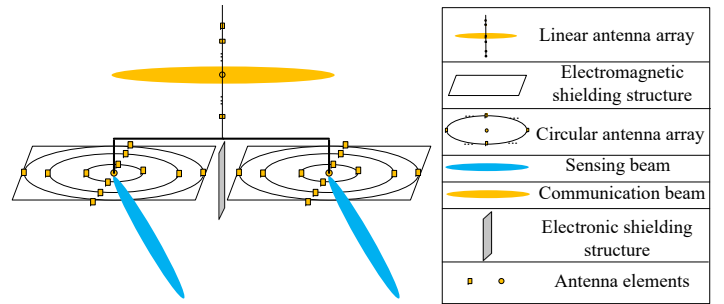


Fig. 2: Design of JSC antenna array

in the three-dimensional (3D) space, where θ denotes the elevation angle and φ denotes the azimuth angle. ComA of each UAV generates ComB with elevation beamwidth³ $\Delta\theta_c$ and azimuth beamwidth $\Delta\phi_c$. SenA of each UAV generates SenB with elevation beamwidth $\Delta\theta_r$ and azimuth beamwidth $\Delta\phi_r$. Then the average directional gain of a 3D beam can be approximated by [11] [22]

$$g \approx \frac{26000}{\Delta\theta \cdot \Delta\phi}, \quad (2)$$

where $\Delta\theta$ and $\Delta\phi$ are the azimuth beamwidth and elevation beamwidth, respectively.

The antenna array designed to achieve beam sharing consists of two parts, as illustrated in Fig. 2. The upper linear subarray is ComA that has M_{com} antenna elements with inter-distance half-wavelength. The lower subarray is SenA composed of two decoupled circular subarrays, where one is transmitting array (TxA) and the other is receiving array (RxA). TxA and RxA are used to generate transmitting SenB and receiving SenB, respectively. The electronic shielding plate is placed between two subarrays of SenA and the pulse response between two subarrays is also accurately measured to eliminate self-interference between TxA and RxA of SenA in real-time manner [23].

³In this paper, the term “beamwidth” refers to the -3dB half-power beamwidth.

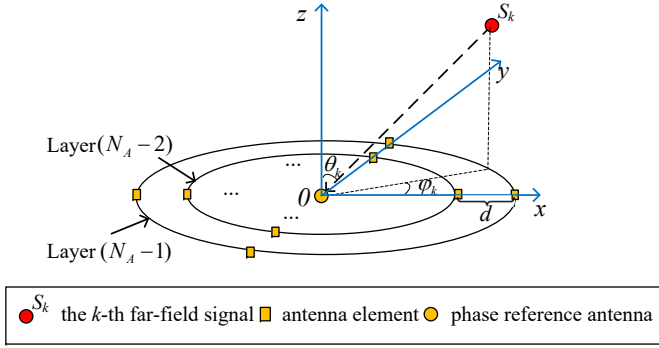


Fig. 3: Design of JSC sensing subarray

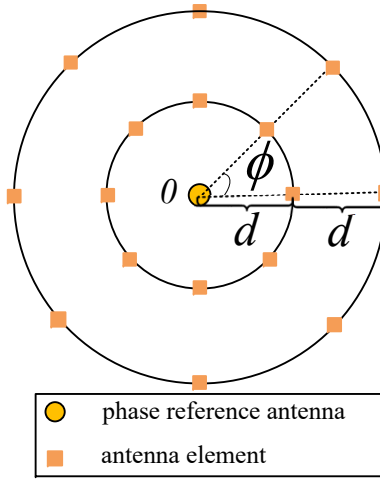


Fig. 4: Design of adjacent layers of JSC sensing subarray

Two subarrays of SenA are used to solve the problem of minimum detection range by achieving simultaneous transmitting and receiving of radar sensing signal [21]. If SenA adopts only one subarray, then it has to arrange time slots for transmitting and receiving the radar signal. In this case, the radar echo can come back to SenA before the slot for receiving, and then the missing of the target will happen. Only when the distance between UAV and the target is larger than the minimum value can the target be possibly detected, which is inapplicable to the situation where the target is close to the JSC units. By contrast, if we adopt double subarrays to form SenA, then the radar sensing signal can be transmitted and received simultaneously. Thus, the problem of minimum detection range is solved.

As illustrated in Fig. 3, SenA has antennas arranged in concentric circles. There are N_A circles in each SenA, and we define each circle as a layer. From center to periphery, SenA has the 0th layer to the $(N_A - 1)$ th layer. Except for the 0th layer with only one antenna element that is the phase reference antenna (PhRefA), there are 2^b antenna elements in each layer, where b is a positive integer.

Fig. 4 shows the adjacent layers of SenA. The distance between the antennas that locate at the same polar angle of adjacent layers is d . Antennas in each layer locate at the evenly

split angles, and are referred to as the 0th to the $(2^b - 1)$ th antenna, anti-clockwise.

C. Beamforming of JSC Antenna Array

1) *Beamforming of SenA*: Assume that there are K_s planar far-field signals arriving at SenA from different directions. The angle of arrival (AoA) of the k th ($k = 1, 2, \dots, K_s$) signal is $\mathbf{p}_k = (\varphi_k, \theta_k)^T$. We use $\Theta = \{\mathbf{p}_1, \dots, \mathbf{p}_{K_s}\}$ to denote the set of AoAs of all K_s signals.

Let $A_{p,q}$ be the q th antenna in the p th layer of SenA. The polar angle of $A_{p,q}$ is $\psi_{p,q} = q \cdot \phi$, where $\phi = \frac{2\pi}{2^b}$. For the k th signal with AoA \mathbf{p}_k , the phase difference between $A_{p,q}$ and PhRefA is given by

$$a_{p,q}(\mathbf{p}_k) = \exp \left\{ -j \frac{2\pi}{\lambda} \mathbf{P}_{p,q}^T \mathbf{v}_k \right\}, \quad (3)$$

where λ is the wavelength, and

$$\mathbf{v}_k = [\cos \varphi_k \sin \theta_k, \sin \varphi_k \sin \theta_k]^T, \\ \mathbf{P}_{p,q} = [p \cdot d \cos(\psi_{p,q}), p \cdot d \sin(\psi_{p,q})]^T.$$

Furthermore, the steering vector of SenA is

$$\mathbf{a}(\mathbf{p}_k) = [1, a_{1,0}(\mathbf{p}_k), \dots, a_{N_A-1,2^b-1}(\mathbf{p}_k)]^T, \quad (4)$$

enumerating the phase differences between the PhRefA and all the other antenna elements of SenA. Then the steering matrix for K_s far-field signals is $\mathbf{A} = [\mathbf{a}(\mathbf{p}_1), \dots, \mathbf{a}(\mathbf{p}_{K_s})]$.

The received signal vector for SenA is

$$\mathbf{y} = \mathbf{A} \mathbf{s}_r + \mathbf{n}_s, \quad (5)$$

where \mathbf{s}_r is the source signal vector of dimension $K_s \times 1$, and \mathbf{n}_s is the additive white Gaussian noise (AWGN) with covariance matrix $\sigma_r^2 \mathbf{I}_{K_s}$ and zero mean.

Based on the least square (LS) error principle, the beamforming problem of SenA can be formulated as [14]

$$\min_{\mathbf{w}_r} \|\mathbf{w}_r^H \mathbf{A} - \mathbf{r}_d^T\|_2^2, \quad (6)$$

where \mathbf{w}_r is the normalized beamforming vector for SenA to generate SenB, and \mathbf{r}_d is the desired response, i.e.,

$$\mathbf{r}_d = \text{diag}(\mathbf{r}_{ad}) \times \mathbf{r}_{pd}, \quad (7)$$

where

$$\mathbf{r}_{ad} = [r_{ad}(\mathbf{p}_1), \dots, r_{ad}(\mathbf{p}_k)]^T, \\ \mathbf{r}_{pd} = [r_{pd}(\mathbf{p}_1), \dots, r_{pd}(\mathbf{p}_k)]^T,$$

representing the desired amplitude response and desired phase response, respectively. Note that \mathbf{r}_{ad} is a column vector of real values, and \mathbf{r}_{pd} is a column vector of complex values with unit modulus.

Two-step iterative LS beamforming method is presented to generate high-performance beam given AoAs [14], as shown in **Algorithm 1**. First, we determine the desired AoAs, amplitude response \mathbf{r}_{ad} and the corresponding steering matrix \mathbf{A} . Then we set the initial beamforming vector as $\mathbf{w}_{r,0} = \mathbf{0}$ and set the iteration time threshold as τ_{th} . If the iteration time m is smaller than τ_{th} , then the phase response \mathbf{r}_{pd} and the beamforming vector $\mathbf{w}_{r,m}$ are updated iteratively. After the iteration time

Algorithm 1: Two-step Iterative LS Beamforming Algorithm

Input: The desired AoAs $\{\mathbf{p}_1, \mathbf{p}_2, \dots, \mathbf{p}_L\}$, and the corresponding steering matrix \mathbf{A} .
The desired amplitude pattern \mathbf{r}_{ad} .
Initial beamforming vector $\mathbf{w}_{r,0}$.
Iteration index $m = 0$.
Iteration time threshold τ_{th} .

Output: Final converged beamforming vector $\mathbf{w}_{r,m}$.

while $\mathbf{w}_{r,m}$ does not converge and $m \leq \tau_{th}$ **do**

- 1) $m = m + 1$.
- 2) $\mathbf{r}_{pd} = [\text{diag}(\mathbf{r}_{ad})]^{-1} \mathbf{A}^T \mathbf{w}_{r,m-1}^*$.
- 3) $\mathbf{r}_{pd1} = \frac{\mathbf{r}_{pd}}{|\mathbf{r}_{pd}|}$.
- 4) $\mathbf{w}_{r,m} = (\mathbf{A}^H)^{\dagger} [\text{diag}(\mathbf{r}_{ad})]^H \mathbf{r}_{pd1}^*$.

end

return $\mathbf{w}_{r,m}$

reaches τ_{th} or $\mathbf{w}_{r,m}$ converges to a stable value, $\mathbf{w}_{r,m}$ is the output as the beamforming vector for SenB beamforming. In **Algorithm 1**, $|\mathbf{x}|$ brings out the vector where the i th entry is the modulus of the i th entry of \mathbf{x} (\mathbf{x} can degrade to scalar), and $\frac{\mathbf{r}_{pd}}{|\mathbf{r}_{pd}|}$ is entry-wise division.

2) *Beamforming of ComA:* Assume that there are K_c planar far-field signals arriving at ComA. The i th signal's AoA is θ_i . Similar to SenA, the steering vector of ComA is

$$\bar{\mathbf{a}}(\theta_i) = \left[1, e^{j\frac{2\pi}{\lambda} d_c \cos \theta_i}, \dots, e^{j\frac{2\pi}{\lambda} (M_{com}-1) d_c \cos \theta_i} \right]^T, \quad (8)$$

where d_c is the distance between the adjacent antennas of ComA. Then we obtain the steering matrix of ComA as $\bar{\mathbf{A}} = [\bar{\mathbf{a}}(\theta_1), \dots, \bar{\mathbf{a}}(\theta_{K_c})]$. Furthermore, the received signal of ComA can be expressed as $\mathbf{y}_c = \bar{\mathbf{A}}\mathbf{s}_c + \mathbf{n}_c$, where \mathbf{s}_c is the source signal vector of dimension $K_c \times 1$, and \mathbf{n}_c is AWGN with covariance matrix $\sigma_c^2 \mathbf{I}_{K_c}$ and zero mean. The objective for the ComA beamforming is given by

$$\min_{\mathbf{w}_c} \left\| \mathbf{w}_c^H \bar{\mathbf{A}} - \bar{\mathbf{r}}_{pd}^T \times \text{diag}(\bar{\mathbf{r}}_{ad}) \right\|_2^2, \quad (9)$$

where $\bar{\mathbf{r}}_{ad}$ and $\bar{\mathbf{r}}_{pd}$ are the desired amplitude response and desired phase response of ComB, respectively. Note that $\bar{\mathbf{r}}_{ad}$ is a column vector of real values, and $\bar{\mathbf{r}}_{pd}$ is a column vector of complex values with unit modulus. **Algorithm 1** is also applied to generate ComB. After τ_{th} iterations or \mathbf{w}_c converges to a stable value, the desired beamforming vector for ComB will be output.

D. Signal Model of the JSC UAV Network

OFDM signal is adopted in the JSC UAV network to exploit its advantage of the frequency diversity and obtain high processing gain [19]. The baseband OFDM JSC signal is modeled as [19]

$$x(t) = \sum_{m=0}^{M_s-1} \sum_{q=0}^{N_c-1} d_{Tx}(mN_c+q) \exp(j2\pi f_q t) \text{rect}\left(\frac{t-mT}{T}\right), \quad (10)$$

where M_s is the number of OFDM symbols in one frame, N_c is the number of subcarriers, $d_{Tx}(mN_c+q)$ is the transmit

symbol on the q th subcarrier of the m th OFDM block, B is the bandwidth of the JSC signal, $f_q = \frac{qB}{N_c}$ is the baseband frequency of the q th subcarrier, and T is the duration time of each OFDM symbol that contains guard interval and the duration of OFDM block.

The phase difference between the transmitted and the received OFDM symbols is used to estimate the Doppler frequency shift and the time delay between the target and the UAV.

The Doppler shift results from the radial relative velocity between the UAV and the target, and can be presented as

$$f_{d,s} = \frac{2v_{rel}f_c}{c_0}, \quad (11)$$

where c_0 is the speed of light, f_c is the carrier frequency of the OFDM signal, and v_{rel} is the radial relative velocity between UAV and the target. The time delay is expressed as

$$\tau_s = \frac{2R_r}{c_0}, \quad (12)$$

where R_r is the distance between the target and the UAV. The complex ratio of the received to the transmitted OFDM signal is expressed as [19]

$$\begin{aligned} (\mathbf{D}_{div})_{m,q} &= \frac{d_{Rx}(mN_c+q)}{d_{Tx}(mN_c+q)} \\ &= (\mathbf{H})_{m,q} \exp(-j2\pi f_q \tau_s) \exp(j2\pi m T f_{d,s}), \end{aligned} \quad (13)$$

where $(\cdot)_{m,q}$ is the entry of a matrix at the m th row and the q th column, $d_{Rx}(mN_c+q)$ is the received OFDM symbol corresponding to $d_{Tx}(mN_c+q)$, and $(\mathbf{H})_{m,q}$ is the complex fading factor for the q th subcarrier of the m th OFDM symbol. The matrix form of (13) is given by

$$(\mathbf{D}_{div})_{m,q} = (\mathbf{H})_{m,q} (\mathbf{k}_D \mathbf{k}_R^T)_{m,q}, \quad (14)$$

where $m = 0, 1, \dots, M_s - 1$, $q = 0, 1, \dots, N_c - 1$, $\mathbf{k}_R(q) = \exp(-j2\pi f_q \tau_s)$, and $\mathbf{k}_D(m) = \exp(j2\pi m T f_{d,s})$.

By applying discrete Fourier transform (DFT) to each column of \mathbf{D}_{div} and inverse discrete Fourier transform (IDFT) to each row of \mathbf{D}_{div} , $f_{d,s}$ and R_r can be obtained respectively.

Let $\mathbf{D}_{m,IDFT}$ denote the IDFT of the m th row of \mathbf{D}_{div} , and $\mathbf{D}_{q,DFT}$ denote the DFT of the q th column of \mathbf{D}_{div} . The index corresponding to the peak of $\mathbf{D}_{m,IDFT}$ depends on $f_{d,s}$ and can be obtained by one-dimensional exhaustive search as follows [4]:

$$ind_{d,m} = \lfloor f_{d,s} T M_s \rfloor, \quad ind_{d,m} = 0, 1, \dots, N_c - 1. \quad (15)$$

Similarly, the index corresponding to the peak of $\mathbf{D}_{q,DFT}$ depends on R_r and can be obtained by one-dimensional exhaustive search as follows [4]:

$$ind_{R,q} = \left\lfloor \frac{2R_r B}{c_0} \right\rfloor, \quad ind_{R,q} = 0, 1, \dots, M_s - 1. \quad (16)$$

Based on (15) and (16), we can obtain $f_{d,s}$ and R_r , respectively. The accuracy of the estimation depends on the duration time of each OFDM symbol and the bandwidth of signal [4]. This radar echo processing technique can generate a processing gain as [4]

$$G_p = N_c M_s. \quad (17)$$

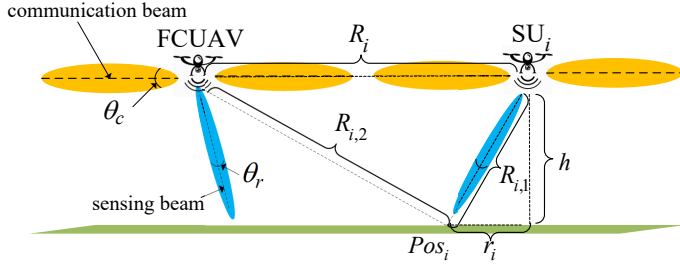


Fig. 5: Front view of vertical pattern of sensing beam and communication beam

E. Modeling of Mutual Sensing Interference

In order to model the mutual sensing interference, the power spectrum of the JSC OFDM signal needs to be considered first, which is the sum of the power spectra of N_c subcarriers [24]. According to [24], the power spectrum of the q th subcarrier is

$$S_q(f') = T_s \left[\frac{\sin(\pi(f'T_s N_c - q))}{\pi(f'T_s N_c - q)} \right]^2, \quad (18)$$

where $T_s = \frac{1}{B}$ is the sampling cycle of the OFDM signal. The aggregate power spectrum of all subcarriers is noise-like [4]. For reasonable simplification, we assume that the transmitting power of the OFDM sensing signal concentrates in the baseband spectrum $[0, B]$. UAVs receive the sensing interference power imposed by all other UAVs' scattered sensing signals.

FCUAV is chosen as the reference to analyze the average sensing interference that a UAV receives from other UAVs. As illustrated in Fig. 5, denote R_i as the distance between SU_i and FCUAV,⁴ Pos_i as the intersection point between the SenB direction of SU_i and SZ of SU_i , $R_{i,1}$ as the distance between SU_i and Pos_i , $R_{i,2}$ as the distance between Pos_i and FCUAV, and r_i as the distance between Pos_i and the projection point of SU_i on SZ. Assuming that the interfering sensing signals are random due to the random scattering, the sensing interfering power imposed by SU_i on FCUAV is formulated as [11], [25]

$$I_{sen,i} = \frac{P_r g_{ts}}{4\pi} R_{i,1}^{-2} \bar{\sigma} \frac{1}{4\pi} R_{i,2}^{-2} \frac{\lambda^2 g_{rs}}{4\pi}, \quad (19)$$

where g_{ts} and g_{rs} are the gains of transmitting and receiving sensing beams respectively, $\bar{\sigma}$ is the mean of radar cross section of target, λ is the wavelength of the carrier of JSC transceiver, and $R_{i,1}$ and $R_{i,2}$ are expressed as follows:

$$\begin{aligned} R_{i,1} &= \sqrt{r_i^2 + h^2}, \\ R_{i,2} &= \sqrt{(R_i - r_i)^2 + h^2}. \end{aligned} \quad (20)$$

The maximal point of $I_{sen,i}$ with regard to r_i is $r_i = \frac{R_i}{2}$, which is easily obtained by the first-order and the second-order derivative of $I_{sen,i}$ versus r_i . Thus, we set $R_{i,1} = R_{i,2} = \left[\left(\frac{R_i}{2} \right)^2 + h^2 \right]^{\frac{1}{2}}$ to obtain the upper bound of the average sensing interference imposed on FCUAV by SU_i .

⁴ R_i is an independently and identically distributed (i.i.d.) variable.

The expectation of sensing interference imposed on FCUAV by M SUs can be upper-bounded by

$$\begin{aligned} I_{sen} &= \sum_{i=1}^M E\{I_{sen,i}\} \\ &= M \times E \left\{ \sum_{i=1}^M \frac{1}{M} \frac{P_r g_{ts} g_{rs}}{4\pi^3} (R_i^2 + 4h^2)^{-2} \lambda^2 \bar{\sigma} \right\}. \end{aligned} \quad (21)$$

The second order derivative of $(R_i^2 + 4h^2)^{-2}$ with regard to R_i is $24R_i^2(R_i^2 + 4h^2)^{-4}$ for $R_i, h > 0$, which is larger than 0. Thus, I_{sen} is convex of R_i for $R_i > 0$. By using the Jensen inequality, we have

$$\begin{aligned} I_{sen} &= \frac{P_r \lambda^2 \bar{\sigma} g_{ts} g_{rs}}{4\pi^3} M \times E \left\{ \sum_{i=1}^M \frac{1}{M} (R_i^2 + 4h^2)^{-2} \right\} \\ &\leq \frac{P_r \lambda^2 \bar{\sigma} g_{ts} g_{rs}}{4\pi^3} \sum_{i=1}^M E \left\{ (R_i^2 + 4h^2)^{-2} \right\}, \end{aligned} \quad (22)$$

where $E \left\{ (R_i^2 + 4h^2)^{-2} \right\}$ can be obtained as

$$E \left\{ (R_i^2 + 4h^2)^{-2} \right\} = \frac{(R_g^2 + 4h^2)^{-1} - (x_Q^2 + 4h^2)^{-1}}{x_Q^2 - R_g^2}. \quad (23)$$

The proof of (23) is given in Theorem 1 in appendix. Then we have

$$I_{sen} = M \frac{P_r \lambda^2 \bar{\sigma} g_{ts} g_{rs}}{4\pi^3} \frac{[(R_g^2 + 4h^2)^{-1} - (x_Q^2 + 4h^2)^{-1}]}{x_Q^2 - R_g^2}. \quad (24)$$

III. SENSING PERFORMANCE ANALYSIS OF THE JSC UAV NETWORK

A. Minimum Required SINR for Effective Sensing

As stated before, the power spectrum of OFDM signal is noise-like. Thus, the interference-and-noise imposed on sensing receiver of each UAV follows the Gaussian distribution, i.e., $A_{in} \sim N(0, N_s + I_{sen})^5$, where N_s is the thermal noise power.

The useful sensing signal power is

$$S = G_p \gamma_s (N_s + I_{sen}), \quad (25)$$

where γ_s denotes SINR of sensing, and G_p is presented in (17). We can obtain the following detection problem:

$$\begin{aligned} H_1 &: y = \sqrt{S} + A_{in} \\ H_0 &: y = A_{in} \end{aligned}, \quad (26)$$

where hypothesis H_1 is that there is a target in the direction of sensing beam, hypothesis H_0 is the opposite, and y is the output signal of radar after processing M_s OFDM symbols.

⁵ $N(\mu, \sigma^2)$ is the Gaussian distribution with μ as mean and σ^2 as variance.

The decision rule of whether there is a target in the sensing direction can be expressed as [20]

$$y \underset{H_0}{\overset{H_1}{\geq}} \eta', \quad (27)$$

where η' is the decision threshold. When $y > \eta'$, the sensor accepts the hypothesis H_1 ; otherwise, the sensor accepts the hypothesis H_0 .

The false alarm rate and the detection probability are the metrics that have to be considered for detection [20], and are presented by

$$P_F = \int_{\eta'}^{\infty} f(y|H_0) dy = Q\left(\frac{\eta'}{\sqrt{N_s + I_{sen}}}\right) \quad (28)$$

and

$$P_D = \int_{\eta'}^{\infty} f(y|H_1) dy = Q\left(\frac{\eta' - \sqrt{S}}{\sqrt{N_s + I_{sen}}}\right), \quad (29)$$

respectively, where $Q(\cdot)$ is the monotonically decreasing Q-function [20]. According to (28), we have

$$\eta' = Q^{-1}(P_F) \sqrt{N_s + I_{sen}}, \quad (30)$$

where $Q^{-1}(\cdot)$ is the inverse function of Q-function. By substituting (25) and (30) into (29), we can obtain P_D as

$$P_D = Q\left[Q^{-1}(P_F) - \sqrt{G_p \gamma_s}\right]. \quad (31)$$

For effective detection, P_F and P_D must be constrained as [20]

$$\begin{cases} P_F \leq \alpha_f \\ P_D \geq \alpha_D \end{cases}, \quad (32)$$

where α_f is the maximum false alarm rate, and α_D is the minimum detection probability. Based on (31) and (32), the minimum SINR to meet the constraints can be expressed as

$$(\text{SINR})_{\min} = \frac{[Q^{-1}(\alpha_f) - Q^{-1}(\alpha_D)]^2}{G_p}. \quad (33)$$

B. Maximum Sensing Range

According to [21], the maximum sensing range of UAV is

$$R_{max}(\beta_R) = \left(\frac{\beta_R P g_{ts} g_{rs} (c_0/f)^2 \bar{\sigma} G_p}{(4\pi)^3 (\text{SINR})_{\min} (kT_0 F_n B + I_{sen}) L_s} \right)^{\frac{1}{4}}, \quad (34)$$

where β_R is SPR, P is the total available radio power, g_{ts} and g_{rs} are the transmitting and the receiving antenna gains of SenB respectively, f is the carrier frequency of transceiver, $\bar{\sigma}$ is the mean radar cross section, L_s is the aggregated power loss at the propagation medium, I_{sen} is given in (24), k is the Boltzmann's constant, F_n is the noise figure of the receiver, B is the bandwidth of JSC transceiver, and $T_0 = 290$ K (in absolute temperature) is the standard temperature.

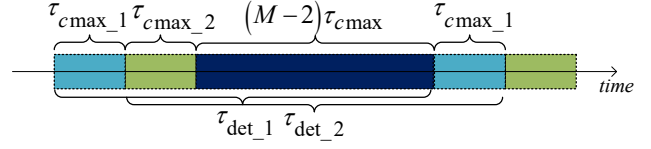


Fig. 6: Time allocation for sensing and communication

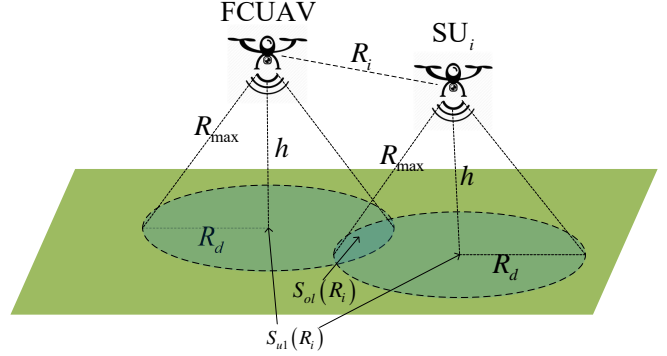


Fig. 7: The illustration of cooperative sensing of the S-C pair

C. Maximum Cooperative Range

The time that SU requires to transmit the sensing data to FCUAV is defined as the ratio of the amount of sensing data to the communication throughput, which is

$$\tau_c(R_i) = \frac{V_{data} \tau_{det}}{T_c(R_i)}, \quad (35)$$

where V_{data} is the generating rate of the sensing data, τ_{det} is the detection time, and $T_c(R_i)$ is the throughput of the communication link between FCUAV and SU_i . With the increase of R_i , $T_c(R_i)$ decreases because the received Comb power decreases.

We adopt TDMA for SUs to transmit the sensing data to FCUAV. Each SU must transmit the sensing data in the assigned time slots of length τ_{cmax} . SUs carry out downward-looking detection constantly and transmit its sensing data in the assigned slots.

Fig. 6 illustrates the time slots allocated to SUs for transmitting sensing data to FCUAV. Let τ_{det_i} and τ_{cmax_i} denote the sensing slots and communication slots for SU_i , respectively. All UAVs are provided with the same sensing time τ_{det} and transmission time τ_{cmax} . In order to ensure the consecutive detection of each UAV, we have

$$\tau_{cmax} = \frac{1}{M} \tau_{det}. \quad (36)$$

In this case, after SU_i completes the sensing tasks in τ_{det_i} , the next slot for SU_i to transmit sensing data comes again.

Based on (35), (36) and $\tau_c \leq \tau_{cmax}$, we obtain $T_c(R_i) \geq M \times V_{data}$. Thus, the distance between FCUAV and each SU is no larger than MCR, i.e.,

$$x_Q = T_c^{-1}(M \times V_{data}), \quad (37)$$

where $T_c^{-1}(\cdot)$ is the inverse function of $T_c(R_i)$ and will be presented in the next section.

D. Cooperative Sensing Performance Analysis

We define an SU and FCUAV that are communicating sensing data as an S-C pair. As shown in Fig. 7, the radius of SZ of each UAV is formulated as

$$R_d = \sqrt{(R_{\max})^2 - h^2} \times [u(R_{\max} - h)], \quad (38)$$

where $u(\cdot)$ is the step function⁶. The overlapped area between SZs of the S-C pair is

$$S_{ol}(R_i) = \left[2R_d^2 \arccos\left(\frac{R_i}{2R_d}\right) - R_i \sqrt{R_d^2 - \left(\frac{R_i}{2}\right)^2} \right] \times u(2R_d - R_i). \quad (39)$$

Then, the union area of SZs of the S-C pair is

$$S_{u1}(R_i) = 2\pi R_d^2 - S_{ol}(R_i). \quad (40)$$

The expectation of $S_{u1}(R_i)$, for $R_g \leq R_i < x_Q$, is defined as the sensing performance metric of the S-C pair, which is formulated as [1]

$$E_S(x_Q) = \int_{R_g}^{x_Q} f_{R_i}(r) S_{u1}(r) dr = \begin{cases} F_1(x_Q), & x_Q < 2R_d \\ F_2(x_Q), & x_Q \geq 2R_d \end{cases}, \quad (41)$$

where $f_{R_i}(r) = \frac{2r}{x_Q^2 - R_g^2}$ for $R_g < r < x_Q$, is the probability density function (PDF) of R_i . Moreover, $F_1(x_Q)$ and $F_2(x_Q)$ are given in (42) and (43), respectively.

There are M S-C pairs located in MCA. ACSA of the JSC UAV network is defined as the average union area of SZs of M S-C pairs. Because it is extremely intractable to obtain an explicit expression of the average union area of a certain number of randomly distributed circle areas. For tractability, we merely subtract the overlapped sensing area between each SU and FCUAV to obtain the upper bound of ACSA (UB-ACSA) as the sensing performance metric of the JSC UAV network. UB-ACSA is obtained as [1]

$$\begin{aligned} \overline{S_u}(M) &= E_{\mathbf{R}} \left\{ \sum_{i=1}^M [S_{u1}(R_i) - S(R_d)] \right\} + S(R_d) \\ &= M \times E_S(x_Q) - (M-1)S(R_d), \end{aligned} \quad (44)$$

where $S(R_d) = \pi R_d^2$ is the area of SZ of each UAV, and $\mathbf{R} = (R_1, R_2, \dots, R_M)$ is the multiple random variables composed of the distances between SUs and FCUAV. Each element of \mathbf{R} is an i.i.d. variable.

UB-ACSA can be achieved when all SUs do not have overlapped SZs, which requires FCUAV to coordinate the trajectory of each SU. The larger UB-ACSA is, the better the sensing performance of the JSC UAV network is. The JSC UAV network can detect the zone with area of UB-ACSA in much shorter time than individual UAV can do. The overlapped SZs of SUs can be detected by different SUs from different directions, which can reduce the probability of false detection in the overlapped SZs.

⁶i.e., when there is $x \geq 0$, $u(x) = 1$; otherwise, $u(x) = 0$.

IV. OUTAGE CAPACITY OF THE JSC UAV NETWORK

In this section, we obtain the outage capacity as the metric of communication performance, as well as the ultimate expression of x_Q with respect to the number of UAVs and SPR.

A. Communication Channel Model

The power of communication signal received by FCUAV is

$$P_0 = P_c g_c h_c x_0^{-\alpha}, \quad (45)$$

where P_c is the power of ComB, α is the path loss exponent, g_c is the directional gain of the communication link, h_c is the small scale fading factor that follows Rician distribution with Rician factor K_h , and x_0 is the distance between the transmitter and FCUAV. We have $g_c = g_{tc} \times g_{rc}$, where g_{tc} and g_{rc} are the directional gains of transmitting ComB and receiving ComB, respectively. The PDF of h_c is expressed as follows [26]:

$$f_{h_c}(w) = \frac{(K_h + 1) e^{-K_h} e^{-\frac{(K_h + 1)w}{\bar{\Omega}}}}{\bar{\Omega}} I_0 \left(2\sqrt{\frac{K_h(K_h + 1)w}{\bar{\Omega}}} \right), \quad (46)$$

where $I_0(x) = \sum_{n=0}^{\infty} \frac{(x/2)^{2n}}{n! \Gamma(n+1)}$ is the 0-th order modified Bessel function of the first kind, $K_h = v^2 / \sigma_K^2$, $\bar{\Omega} = 2\sigma_K^2 + v^2$ is the normalized power, v^2 denotes the strong line-of-sight (LOS) power, and σ_K^2 represents the multipath reflected power [27]–[29].

B. Successful Transmission Probability and Outage Capacity

The successful transmission probability (STP) is defined as the probability that the received SNR (or SINR) is larger than a threshold γ that is necessary for successful transmission [26], [30], i.e.,

$$\begin{aligned} \rho_c^s(x_0, \gamma) &= \Pr \left(\frac{P_0}{N_{com}} > \gamma \right) \\ &= \Pr \left(h_c > \frac{\gamma N_{com}}{P_c g_c} x_0^\alpha \right), \end{aligned} \quad (47)$$

where N_{com} is AWGN of communication receiver. Since h_c follows Rician distribution with Rician factor K_h , STP is formulated as [27]

$$\rho_c^s(x_0, \gamma) = Q \left(\sqrt{2K_h}, \sqrt{\frac{2\gamma(1+K_h)x_0^\alpha N_{com}}{g_c P_c}} \right), \quad (48)$$

where $Q(a_1, a_2)$ is the first order Marcum Q-function. The outage probability is the complement of ρ_c^s , i.e.,

$$\rho_c^{out} = 1 - \rho_c^s(x_0, \gamma). \quad (49)$$

The outage capacity is written as [30]

$$T_C(x_0) = B(1 - \varepsilon) \log(1 + \gamma_{th}), \quad (50)$$

where B is the available bandwidth of the JSC transceiver, ε is the maximum of ρ_c^{out} , and γ_{th} is the SNR threshold that makes the outage probability equal to ε [30]. If $\gamma > \gamma_{th}$, then

$$F_1(x_Q) = \frac{1}{4(x_Q^2 - R_g^2)} \left\{ x_Q \sqrt{4R_d^2 - x_Q^2} (2R_d^2 + x_Q^2) + 8\pi R_d^2 x_Q^2 + 8R_d^2 \left[R_g^2 \arccos\left(\frac{R_g}{2R_d}\right) - x_Q^2 \arccos\left(\frac{x_Q}{2R_d}\right) \right] \right. \\ \left. + 8R_d^4 \left[2 \arcsin\left(\frac{R_g}{2R_d}\right) + \operatorname{arccot}\left(\frac{\sqrt{4R_d^2 - x_Q^2}}{x_Q}\right) - \operatorname{arccot}\left(\frac{\sqrt{4R_d^2 - R_g^2}}{R_g}\right) - 2 \arcsin\left(\frac{x_Q}{2R_d}\right) \right] \right. \\ \left. - R_g \sqrt{4R_d^2 - R_g^2} (2R_d^2 + R_g^2) - 8\pi R_d^2 R_g^2 \right\}. \quad (42)$$

$$F_2(x_Q) = \frac{1}{x_Q^2 - R_g^2} \left\{ 2\pi R_d^2 (x_Q^2 - R_g^2) + \pi R_d^4 - 2R_d^4 \operatorname{arccot}\left(\frac{\sqrt{4R_d^2 - R_g^2}}{R_g}\right) \right. \\ \left. - 2R_d^2 \arccos\left(\frac{R_g}{2R_d}\right) (2R_d^2 - R_g^2) - \frac{1}{4} R_g \sqrt{4R_d^2 - R_g^2} [2R_d^2 + R_g^2] \right\}. \quad (43)$$

the outage probability will be larger than ε . Combining (48), (49) and (50), we have

$$T_c(x_0) = B(1 - \varepsilon) \log \left(1 + \frac{g_c P_c [Q^{-1}(\sqrt{2K_h}, 1 - \varepsilon)]^2}{2(1 + K_h) x_0^\alpha N_{com}} \right), \quad (51)$$

where $Q^{-1}(\cdot, \cdot)$ is the inverse function of $Q(a_1, a_2)$ with regard to a_2 ,⁷ and $T_c(x_0)$ is the communication performance metric of the JSC UAV network.

According to (37) and (51), we can obtain x_Q as

$$x_Q = \left[\frac{g_c(1 - \beta_R)P [Q^{-1}(\sqrt{2K_h}, 1 - \varepsilon)]^2}{2(1 + K_h)N_{com} \left(2^{\frac{M V_{data}}{B(1 - \varepsilon)}} - 1 \right)} \right]^{1/\alpha}. \quad (52)$$

With (41), (42), (43), (44) and (52), UB-ACSA of the JSC UAV network can be calculated as the function of M and β_R .

V. NUMERICAL RESULTS

In this section, numerical and Monte-Carlo simulations are conducted to verify the theoretical analysis in the previous sections and show the impact of the number of SUs and SPR on UB-ACSA. The parameters used in the simulations are listed in TABLE II [21], [29], [32].

Fig. 8 shows the normalized 3D beam pattern of SenB. The mainlobe gain of 3D SenB is at least 21dB higher than that of the sidelobes. The azimuth and elevation beamwidth of SenB are approximately 4.5 and 5 degrees, respectively. Therefore, the average gain of SenB is approximately 128 (in decimal), based on (2).

Fig. 9 shows the normalized 2D beam pattern of ComA. The mainlobe gain of ComB is at least 15 dB higher than that of the sidelobes. The elevation beamwidth of ComB is approximately 9 degrees. Besides, the azimuth beamwidth of

TABLE II: Simulation Parameters

Parameter Items	Value	Description
P	10 W	The total available power
N_{com}	- 94 dB	The power of AWGN for communication
γ	2	The threshold for STP
g_{tc}	8	The gain of transmitting ComB
g_{rc}	8	The gain of receiving ComB
M_s	16	The number of OFDM symbols in a frame
N_c	64	The number of subcarriers
G_p	1024	The processing gain of sensing
M_{com}	16	The number of antennas of ComA
N_A	17	The number of layers of SenA
2^b	16	The number of antennas in each layer of SenA
α_f	10^{-8}	The maximum false alarm rate
α_D	0.99999999	The minimum detection probability
h	150 m	The flying height of UAVs
α	2.6	The path loss exponent
ε	0.1	The maximum outage probability
f_c	24 GHz	The carrier frequency
$\bar{\sigma}$	1	The average radar cross section
F_n	10	The noise figure of receiver
T_0	290 K	The standard temperature
B	100 MHz	The bandwidth of transceiver
V_{data}	1 MB/s	The generating rate of sensing data
K_h	10 dB	The Rician factor
L_s	1	The propagation loss

⁷As $Q(a_1, a_2)$ is a monotonically decreasing function of a_2 [31], the inverse function of the first order Marcum Q-function with regard to a_2 exists. If $b_1 = Q^{-1}(\sqrt{2K_h}, 1 - \varepsilon)$, then $Q(\sqrt{2K_h}, b_1) = 1 - \varepsilon$.

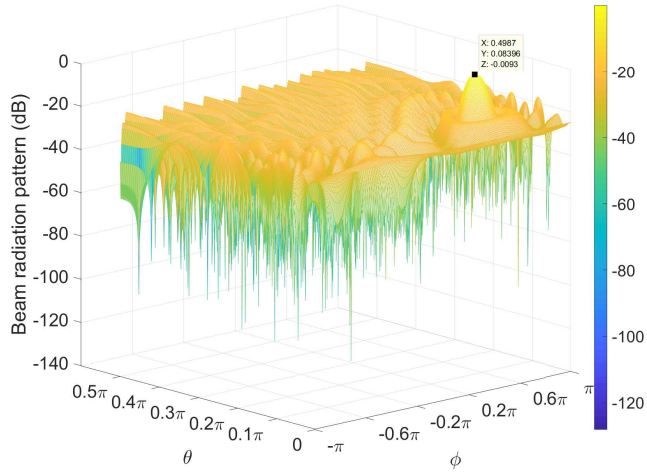


Fig. 8: 3D beam radiation pattern of SenB over AoAs in radians

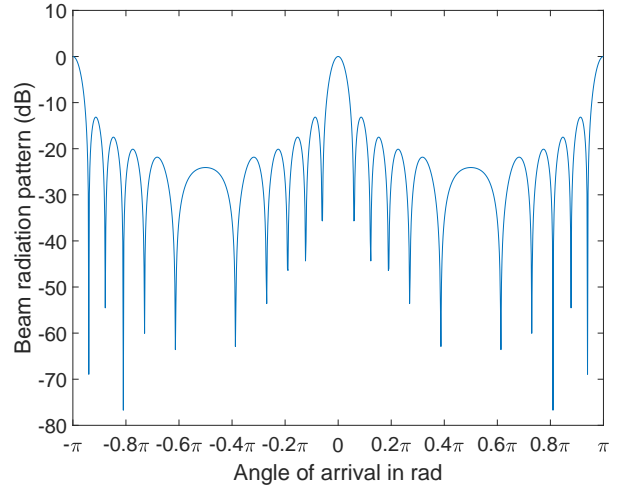


Fig. 9: Beam radiation pattern of ComB over AoAs in radians

ComB is 360 degrees. Thus, the average gain of ComB is approximately 8 (in decimal) according to (2).

Fig. 10 plots both analytical and simulation results of STP versus the transmission distance under different SPR. We can see that STP is a monotonically decreasing function of the transmission distance. We also see the transmission distance becomes smaller with the increase of SPR under the same STP constraint, because the ComB power decreases as SPR or transmission distance increases.

Fig. 11 presents the results of P_D versus β_R and M . The target is at the distance of $R_{max} = 500$ m, and the maximum false alarm rate is $\alpha_f = 10^{-8}$. As is shown in Fig. 11, on the one hand, P_D decreases sharply when M increases to a certain value under given β_R . This is because the increase of M results in the decrease of x_Q and the increase of I_{sen} . On the other hand, when M is given, P_D first increases with the increase of β_R . Then after the maximum point, P_D decreases. This is because as β_R increases, the power of SenB increases at first, increasing the SINR of sensing. After β_R gets too large, the ComB power decreases, leading to the decrease of x_Q and increase of I_{sen} . Thus, when SINR of sensing is lower than $(\text{SINR})_{\min}$, P_D will decrease sharply with the deterioration of SINR. The decrease of R_{max} is required to increase SINR of sensing when β_R or M increases.

Fig. 12 plots both the analytical and simulation results of UB-ACSA changing versus β_R , under different given M . Each curve can be generally divided into three stages given M . In the first stage where β_R is low, the power of ComB is large. Then MCA is large enough for UAVs to expand the sensing zone. Thus, UB-ACSA increases with the increase of β_R . When β_R is too large, the second stage comes. In the second stage, after the maximum point, UB-ACSA decreases with the increase of β_R , because the mutual sensing interference (i.e., I_{sen}) will increase with the decrease of x_Q and the increase of the SenB power. Therefore, the maximum sensing range (i.e., R_{max}) decreases with the increase of β_R in the second

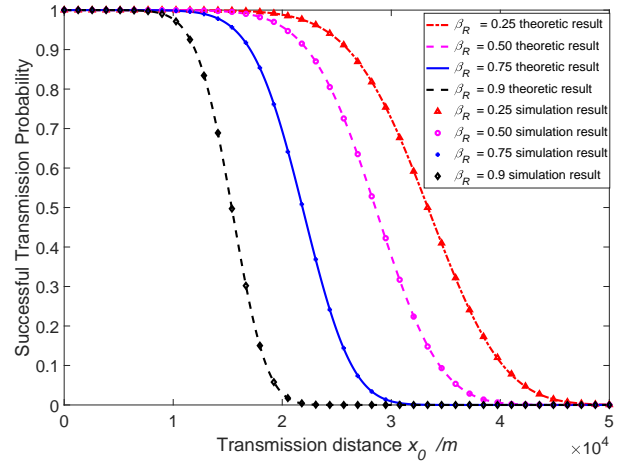


Fig. 10: STP decreases with transmission distance increasing under different SPRs when $K_h = 10$

stage. When β_R is so large that $R_{max} < h$ holds, the third stage appears. In the third stage, UB-ACSA decreases and converges to 0 m², because I_{sen} is extremely large. Thus, in the third stage, it would be better to only deploy FCUAV to carry out the sensing mission than to deploy any other SUs. In Fig. 12, when the JSC UAV network contains 100 SUs, the maximum UB-ACSA is 8.32×10^8 m², which is achieved when there is $\beta_R = 0.5430$. With the above procedure, we can determine the optimal β_R for each UAV given M .

Fig. 13 demonstrates the analytical and simulation results of UB-ACSA changing versus M under different β_R . Each curve of UB-ACSA has three obvious stages. In the first stage where M is relatively small, UB-ACSA increases with the increase of M fast and linearly. This results from that x_Q is considerably large, because the communication capacity requirement for integrating the SUs' sensing data is low. When M gets too large, the second stage comes, where x_Q is much smaller.

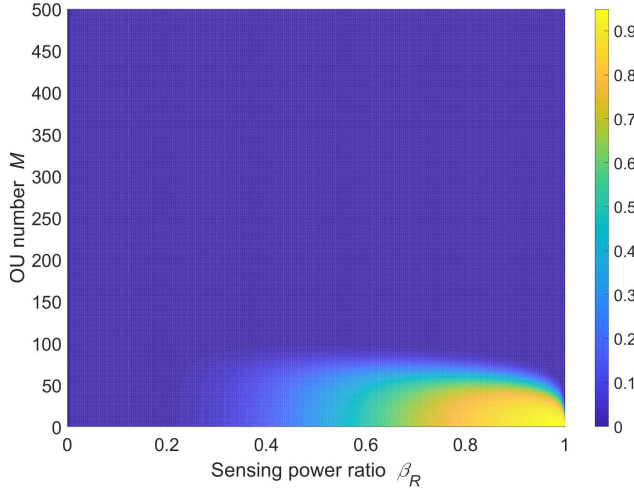


Fig. 11: P_D decreases with the increase of SPR and SU number when $K_h = 10$, $R_{max} = 500$ m, and $\alpha_f = 10^{-8}$

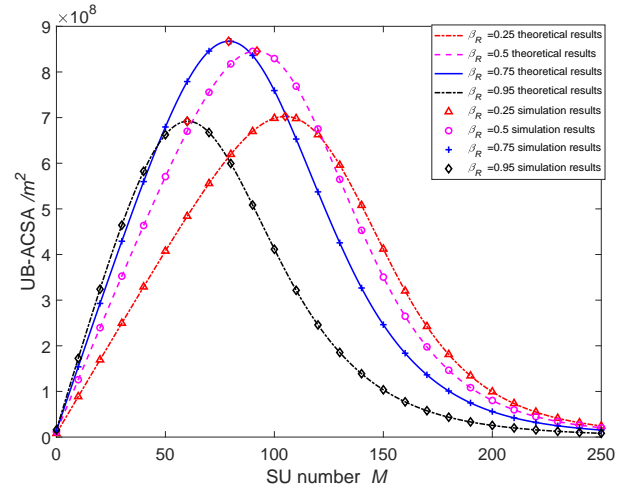


Fig. 13: UB-ACSA changes against SU number M under different SPR β_R when $K_h = 10$

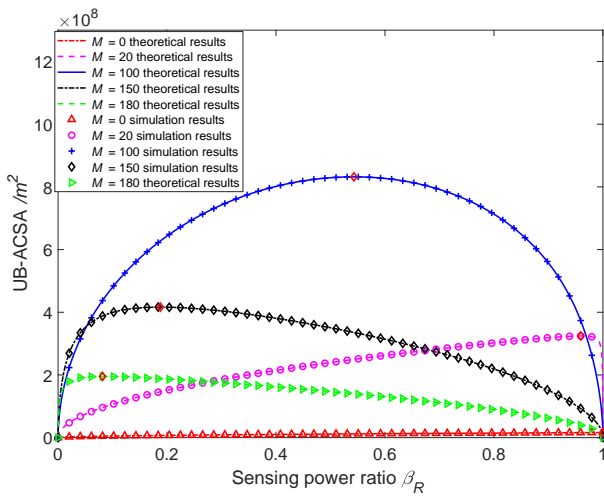


Fig. 12: UB-ACSA changes against SPR β_R under different SU number M when $K_h = 10$

After reaching the maximum point of UB-ACSA, UB-ACSA decreases fast with the increase of M , because x_Q keeps dropping down, I_{sen} gets larger fast, and the overlapped SZs get increasingly larger. If M is so large that x_Q gets extremely small and I_{sen} becomes too large, then R_d converges to 0 m. Therefore, UB-ACSA will become 0 m² hereafter, which is the third stage. Moreover, fewer SUs are needed to reach the maximum UB-ACSA as β_R increases, because if the given ComB power decreases, then fewer SUs can be supported to transmit the entire sensing data to FCUAV. Besides, fewer SUs can make R_d be 0 m as β_R increases, because the increase of the SenB power and decrease of x_Q lead to the increase of I_{sen} . In Fig. 13, when β_R is 0.75, the optimal value of M is 79, which makes UB-ACSA reach the maximum value, i.e., 8.672×10^8 m². Using the above procedure, we can easily

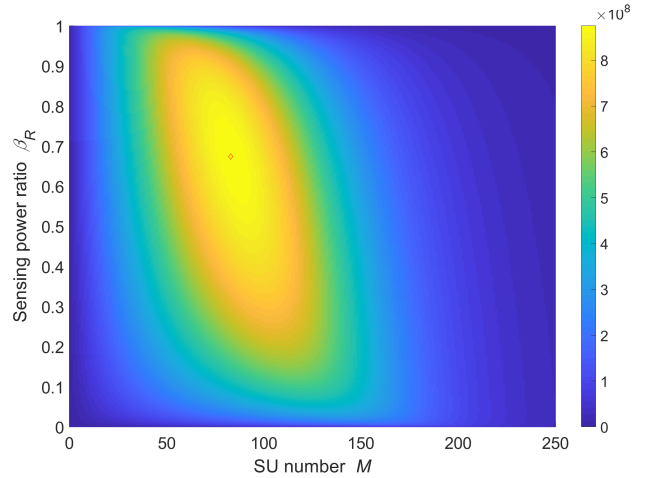


Fig. 14: UB-ACSA changes against SPR β_R and SU Number M when $K_h = 10$

find the optimal M to accomplish the maximum UB-ACSA, given the value of β_R .

Fig. 14 presents the results of UB-ACSA changing versus β_R and M . On the one hand, when β_R and M are relatively small, the communication capacity is much larger than the requirement for sensing data integration, because the ComB power is considerably large, while the number of UAVs to integrate sensing data is too small. Therefore, the communication capacity for data integration is not completely exploited, i.e., UB-ACSA cannot reach the maximum value when β_R and M is small. On the other hand, too large β_R will result in the decrease of UB-ACSA because of the decrease of x_Q . When M is too large, x_Q also becomes quite small, and I_{sen} will become large enough to make R_{max} decrease to a small value. As a result, when M and β_R are too large, UB-ACSA will decrease with the increase of M and β_R until UB-ACSA

reduces to 0 m². In Fig. 14, when $\beta_R = 0.6741$ and $M = 83$, UB-ACSA reaches the maximum value of 8.748×10^8 m². In the above procedure, we can easily determine the optimal values of β_R and M to achieve the optimal UB-ACSA.

VI. CONCLUSION

This work has put forward the average cooperative sensing area as performance metric of cooperative sensing in JSC UAV network. To achieve cooperative sensing of UAV network, we propose a novel design of JSC antenna array that consists of the communication subarray and sensing subarray and put forward relative beamforming algorithm. Further, the upper bound of mutual interference of sensing, the minimum required sensing SINR, the maximum sensing range and the maximum cooperative range that can allow SUs to transmit the sensing data to FCUAV successfully are derived. Further, the upper bound of average cooperative sensing area is derived as the tractable performance metric of cooperative sensing, which is related to SPR and the number of UAVs. SPR determines the maximum sensing range, the upper bound of mutual interference of sensing and the maximum cooperative range. The number of SUs determines the maximum cooperative range and the mutual interference of the sensing of UAVs. Finally, the optimal value of SPR and the number of UAVs to achieve the maximum UB-ACSA have been numerically determined. The results can guide the configuration of the JSC UAV cooperative sensing network.

APPENDIX

Theorem 1. A 2D uniform point process is generated within a concentric circle area whose inner radius and outer radius are R_g and x_Q , respectively. The distance between a generated point and the center is denoted by R_i . Let h denote a constant parameter. Then the expectation of $(R_i^2 + 4h^2)^{-2}$ of R_i is

$$E \left\{ (R_i^2 + 4h^2)^{-2} \right\} = \frac{[(R_g^2 + 4h^2)^{-1} - (x_Q^2 + 4h^2)^{-1}]}{x_Q^2 - R_g^2}.$$

Proof. The cumulative density function of R_i should be $F_{R_i}(r) = \frac{r^2 - R_g^2}{x_Q^2 - R_g^2} (R_g < r < x_Q)$. Thus, the cumulative distribution function of $Y = (R_i^2 + 4h^2)^{-2}$ ($h > 0$ and $R_g < R_i < x_Q$) is

$$\begin{aligned} F_Y(y) &= \Pr(Y \leq y) \\ &= \Pr(R_i^2 \geq y^{-\frac{1}{2}} - 4h^2) \\ &= \Pr\left(R_i \geq \left(y^{-\frac{1}{2}} - 4h^2\right)^{\frac{1}{2}}\right) \\ &= 1 - \frac{\left(y^{-\frac{1}{2}} - 4h^2\right) - R_g^2}{x_Q^2 - R_g^2}, \end{aligned} \quad (53)$$

where $(x_Q^2 + 4h^2)^{-2} \leq y \leq (R_g^2 + 4h^2)^{-2}$. Then, the probability density function of Y is

$$f_Y(y) = \frac{d[F_Y(y)]}{dy} = \frac{1}{2(x_Q^2 - R_g^2)} y^{-\frac{3}{2}}, \quad (54)$$

where $(x_Q^2 + 4h^2)^{-2} \leq y \leq (R_g^2 + 4h^2)^{-2}$. Thus, the expectation of Y is

$$\begin{aligned} E(Y) &= \int_{(x_Q^2 + 4h^2)^{-2}}^{(R_g^2 + 4h^2)^{-2}} y f_Y(y) dy \\ &= \frac{1}{x_Q^2 - R_g^2} \left[(R_g^2 + 4h^2)^{-1} - (x_Q^2 + 4h^2)^{-1} \right]. \end{aligned} \quad (55)$$

□

REFERENCES

- [1] X. Chen, Z. Wei, Z. Fang, H. Ma, Z. Feng, and H. Wu, "Performance of joint radar-communication enabled cooperative UAV network," *IEEE International Conference on Signal, Information and Data Processing 2019*, pp. 1–4, Dec. 2019.
- [2] W. L. Teacy, J. Nie, S. McClean, and G. Parr, "Maintaining connectivity in UAV swarm sensing," *2010 IEEE Globecom Workshops*, pp. 1771–1776, Jan. 2011.
- [3] L. Han and K. Wu, "Joint wireless communication and radar sensing systems- state-of-the-art and future prospects," *IET Microwaves, Antennas & Propagation*, vol. 7, no. 11, pp. 876–885, Aug. 2013.
- [4] C. Sturm and W. Wiesbeck, "Waveform design and signal processing aspects for fusion of wireless communications and radar sensing," *Proceedings of the IEEE*, vol. 99, no. 7, pp. 1236–1259, May. 2011.
- [5] A. Gupta and R. K. Jha, "A survey of 5G network: Architecture and emerging technologies," *IEEE Access*, vol. 3, pp. 1206–1232, May. 2015.
- [6] J. Moghaddasi and K. Wu, "Multifunctional transceiver for future radar sensing and radio communicating data-fusion platform," *IEEE Access*, vol. 4, pp. 818–838, Feb. 2016.
- [7] J. Ellinger, Z. Zhang, Z. Wu, and M. C. Wicks, "Dual-use multicarrier waveform for radar detection and communication," *IEEE Transactions on Aerospace and Electronic Systems*, vol. 54, no. 3, pp. 1265–1278, June 2018.
- [8] C. Shi, F. Wang, M. Sellathurai, J. Zhou, and S. Salous, "Power minimization-based robust OFDM radar waveform design for radar and communication systems in coexistence," *IEEE Transactions on Signal Processing*, vol. 66, no. 5, pp. 1316–1330, Jan. 2018.
- [9] F. Liu, C. Masouros, A. Li, H. Sun, and L. Hanzo, "MU-MIMO communications with MIMO radar: From co-existence to joint transmission," *IEEE Transactions on Wireless Communications*, vol. 17, no. 4, pp. 2755–2770, Feb. 2018.
- [10] P. M. McCormick, S. D. Blunt, and J. G. Metcalf, "Simultaneous radar and communications emissions from a common aperture, Part I: Theory," *2017 IEEE Radar Conference*, pp. 1685–1690, Jun. 2017.
- [11] M. A. Richards, "Fundamentals of radar signal processing," *Tata McGraw-Hill Education*, 2005.
- [12] R. A. Monzingo and T. W. Miller, "Introduction to adaptive arrays," *Scitech publishing*, 2004.
- [13] O. L. Frost, "An algorithm for linearly constrained adaptive array processing," *Proceedings of the IEEE*, vol. 60, no. 8, pp. 926–935, 1972.
- [14] Z. Shi and Z. Feng, "A new array pattern synthesis algorithm using the two-step least-squares method," *IEEE signal processing letters*, vol. 12, no. 3, pp. 250–253, Mar. 2005.
- [15] M. I. Skolnik, "Radar handbook," *McGraw-Hill*, 1970.
- [16] W. M. Z. W. Zhiping Zhang, N. Michael J, "Bio-inspired RF steganography via linear chirp radar signals," *IEEE Communications Magazine*, vol. 54, no. 6, pp. 82–86, June 2016.
- [17] A. G. Stove, "Linear FMCW radar techniques," *Radar and Signal Processing, IEE Proceedings F*, vol. 139, no. 5, pp. 343–350, Oct. 1992.
- [18] F. E. Nathanson, J. P. Reilly, and M. N. Cohen, "Radar design principles- signal processing and the environment," *NASA STI/Recon Technical Report A*, vol. 91, 1991.
- [19] C. Sturm, T. Zwick, W. Wiesbeck, and M. Braun, "Performance verification of symbol-based OFDM radar processing," *2010 IEEE Radar Conference*, pp. 60–63, May 2010.
- [20] B. C. Levy, "Principles of signal detection and parameter estimation," *Springer Science & Business Media*, 2008.
- [21] M. A. Richards, J. Scheer, W. A. Holm, and W. L. Melvin, "Principles of modern radar," *Citeseer*, 2010.
- [22] R. J. Mailloux, *Phased array antenna handbook*. Artech house, 2017.

- [23] Z. Zhang, X. Chai, K. Long, A. V. Vasilakos, and L. Hanzo, "Full duplex techniques for 5G networks: self-interference cancellation, protocol design, and relay selection," *IEEE Communications Magazine*, vol. 53, no. 5, pp. 128–137, May 2015.
- [24] J. G. Proakis, M. Salehi, N. Zhou, and X. Li, "Communication systems engineering," *Prentice Hall New Jersey*, vol. 2, 1994.
- [25] A. F. Molisch, "Wireless communications," *John Wiley & Sons*, vol. 34, 2012.
- [26] X. Yuan, Z. Feng, W. Xu, W. Ni, J. A. Zhang, Z. Wei, and R. P. Liu, "Capacity analysis of UAV communications: Cases of random trajectories," *IEEE Transactions on Vehicular Technology*, vol. 67, no. 8, pp. 7564–7576, Aug. 2018.
- [27] M. M. Azari, F. Rosas, K.-C. Chen, and S. Pollin, "Ultra reliable UAV communication using altitude and cooperation diversity," *IEEE Transactions on Communications*, vol. 66, no. 1, pp. 330–344, Jan. 2018.
- [28] N. Goddemeier and C. Wietfeld, "Investigation of air-to-air channel characteristics and a UAV specific extension to the Rice model," *2015 IEEE Globecom Workshops*, pp. 1–5, Dec. 2015.
- [29] A. A. Khuwaja, Y. Chen, N. Zhao, M.-S. Alouini, and P. Dobbins, "A survey of channel modeling for UAV communications," *IEEE Communications Surveys & Tutorials*, Jul. 2018.
- [30] S. Zhalehpour, M. Uysal, O. A. Dobre, and T. Ngatched, "Outage capacity and throughput analysis of multiuser FSO systems," *2015 IEEE 14th Canadian Workshop on Information Theory*, Jul. 2015.
- [31] D. A. Shnidman, "The calculation of the probability of detection and the generalized marcum Q-function," *IEEE Transactions on Information Theory*, vol. 35, no. 2, pp. 389–400, Mar. 1989.
- [32] V. Lakshmanan, "Overview of radar data compression," *Satellite Data Compression, Communications, and Archiving III*, vol. 6683, Sep. 2007.